Synthesis and Photoluminescence of Three Bismuth(III)-Organic Compounds Bearing Heterocyclic N-Donor Ligands

Alyssa K. Adcock,[a,†] R. Lee Ayscue III,[a, †] Leticia M. Breuer,[a] Chloe P. Verwiel,[a] Alexander C. Marwitz,[a] Jeffery A. Bertke,[a] Valérie Vallet,[b] Florent Réal, [b] and Karah E. Knope[,a]*

[a] Department of Chemistry, Georgetown University, 37th and O Streets, NW, Washington, D.C. 20057, USA.

[b] Université Lille, CNRS, UMR 8523-PhLAM-Physique des Lasers, Atomes et Molécules, F-59000 Lille, France

Supporting Information

I. CRYSTALLOGRAPHIC REFINEMENT DETAILS 2
II. POWDER X-RAY DIFFRACTION PATTERNS 4
III. LUMINESCENCE MEASUREMENTS 7
IV. UV-VIS ABSORPTION SPECTROSCOPY 10
V. THERMOGRAVIMETRIC ANALYSIS 11
VI. RAMAN SPECTRA 14
VII. COMPUTATIONAL ANALYSIS 15

I. Crystallographic Refinement Details

Single crystals of each compound were mounted in Paratone-N oil on a Mitegen micromount, and placed under a cold nitrogen stream prior to data collection. All single crystal data were collected on a Bruker D8 Quest equipped with a Photon100 CMOS detector and a Mo IμS source. Data were collected using a combination of phi and omega scans, and integrated with the Bruker SAINT program. Structure solutions were performed using the SHELXTL software suite. Intensities were corrected for Lorentz and polarization effects, and an empirical absorption correction was applied using SADABS v2014/4. Non-hydrogen atoms were refined with anisotropic thermal parameters, and hydrogen atoms were included in idealized positions unless otherwise noted.

$[Bi_4Cl_8(PDC)_2(phen)_4]\cdot 2MeCN$ (1).

All crystals of compound **1** examined exhibited non-merohedral twinning. Two distinct cells were identified using APEX3 and Cell_Now. Data were integrated and filtered for statistical outliers using SAINT then corrected for absorption by integration using SAINT/TWINABS v2014/2 to sort, merge, and scale the combined data. Combined unit cell parameters were determined from both components using SAINT. The twin law by rows was (-1 0 0), (0 -1 -0.224), (0.025 0 1). Non-overlapping reflections from the primary orientation were used for phasing. Due to a high degree of overlap between reflections of the two domains, inclusion of reflections from the secondary domain resulted in a poor model. Thus, only reflections from the primary domain were used to refine the structure. The primary orientation still contains over 96% completeness; thus, a reliable model could be determined from only the first domain. One acetonitrile was modeled in the outer coordination sphere; one acetonitrile solvent molecule that was disordered across a symmetry site was squeezed from the refinement. The electron count from the "squeeze" model converged in good agreement with the number of solvate molecules predicted by the complete refinement. Phenanthroline and PDC H atoms were included as riding idealized contributors; the H atom U's were assigned as 1.2 times carrier U_{eq}.

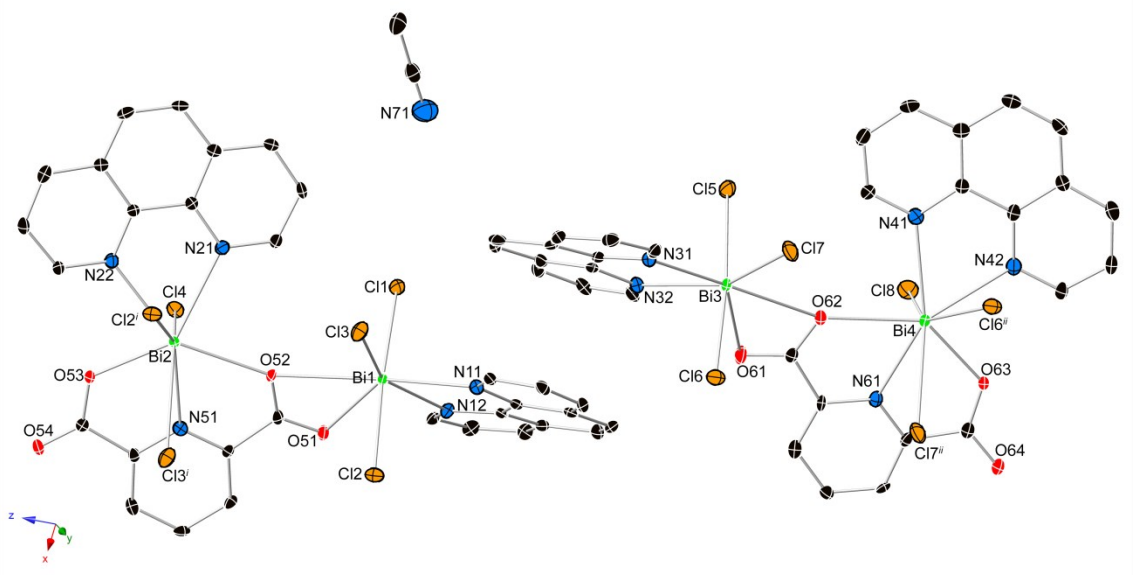

Figure S1. Thermal ellipsoid plot of **1**. Ellipsoids are shown at 50% probability. Green, orange, blue, red, and black spheres represent bismuth, chlorine, nitrogen, oxygen, and carbon atoms, respectively. Symmetry operators: (i) 2 - x, 1 - y, 1 - z; (ii) 1 - x, 1 - y, -z.

$[BiCl_3(phen)_2]$ (2). Phenanthroline H atoms were included as riding idealized contributors; the H atom U's were assigned as 1.2 times carrier U_{eq}. The most disagreeable reflections (110) and (100) were likely affected by the beamstop, and as such, omitted.

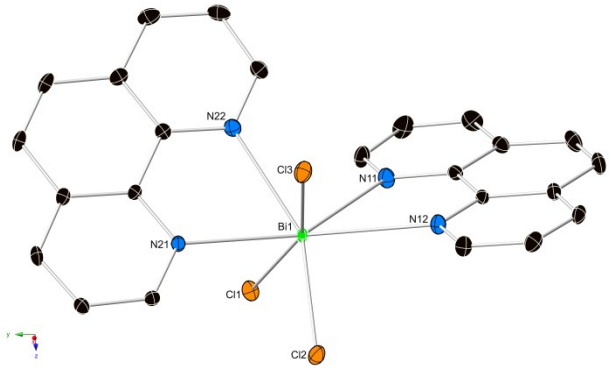

Figure S2. Thermal ellipsoid plot of **2**. Ellipsoids are shown at 50% probability. Green, orange, blue, and black spheres represent bismuth, chlorine, nitrogen, and carbon atoms, respectively.

$[Bi_2Cl_6(terpy)_2]$ (3). Terpyridine H atoms were included as riding idealized contributors; the H atom U's were assigned as 1.2 times carrier U_{eq}. The most disagreeable reflection (011) was omitted.

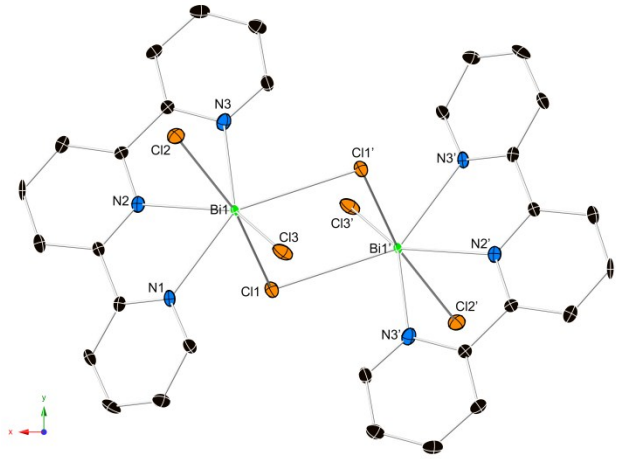

Figure S3. Thermal ellipsoid plot of **3**. Ellipsoids are shown at 50% probability. Green, orange, blue, and black spheres represent bismuth, chlorine, nitrogen, and carbon atoms, respectively. Symmetry operators: (i) -x, -y + 1, -z + 1.

II. Powder X-Ray Diffraction Patterns

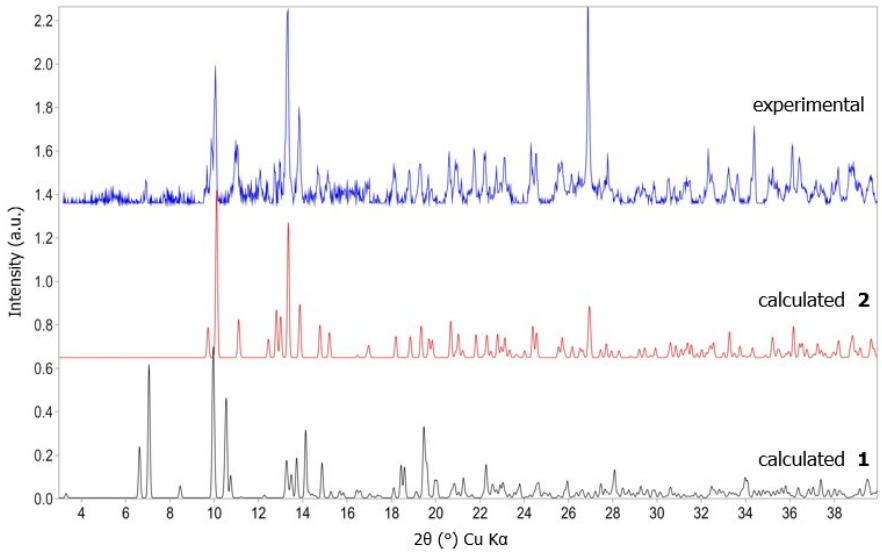

Figure S4. Powder X-ray diffraction data for the bulk reaction from which single crystals of **1** and microcrystalline powder of **2** were observed.

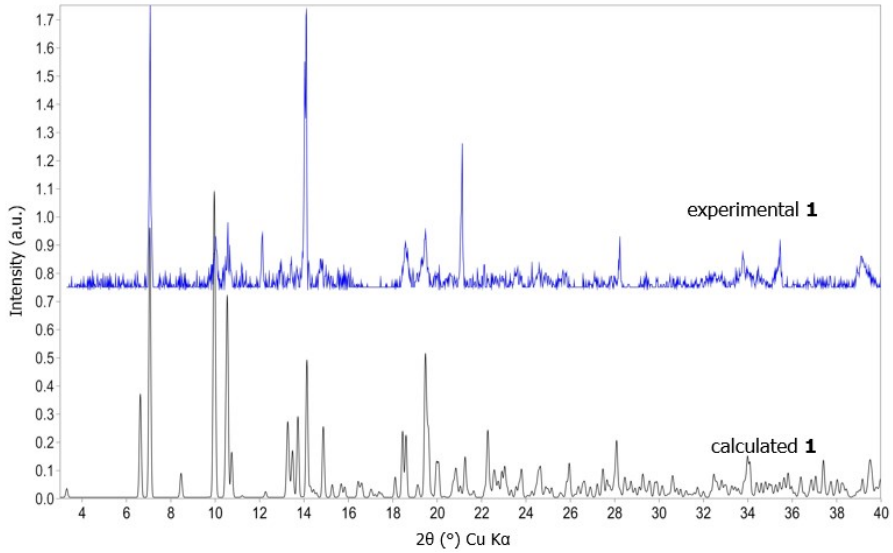

Figure S5. Powder X-ray diffraction data for the manually separated product of **1**. Agreement between the calculated pattern generated from the crystallographic information file and the experimental data as well as the elemental analysis results are consistent with phase purity of the manually separated phase.

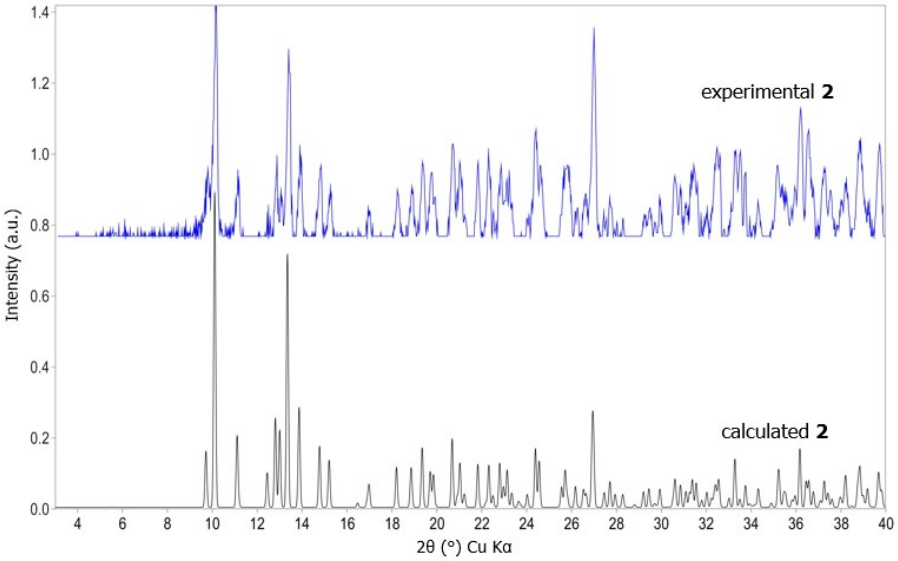

Figure S6. Powder X-ray diffraction data for the bulk product obtained following the synthetic procedure outlined by Bowmaker et al.[10]

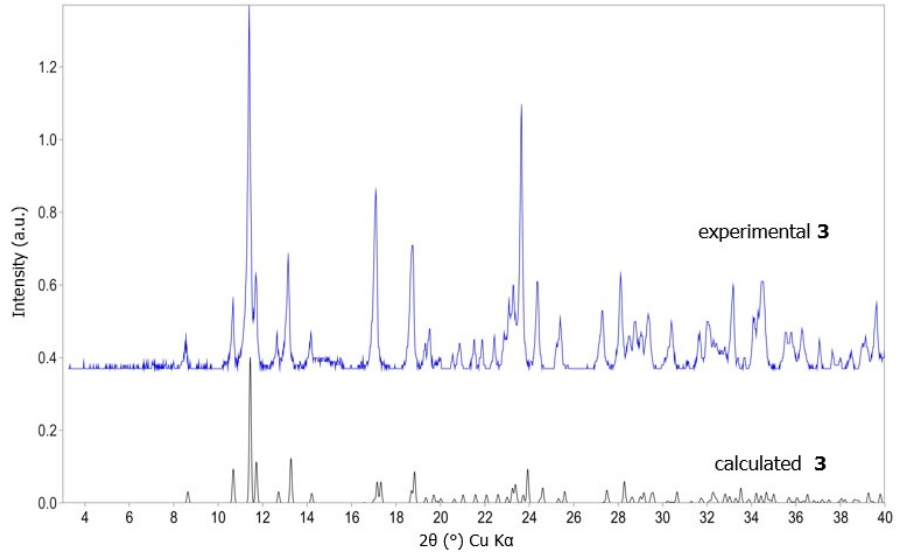

Figure S7. Powder X-ray diffraction data for the bulk product from which **3** was isolated. Agreement between the calculated pattern generated from the crystallographic information file and the experimental data support that the crystal used for structure determination is representative of the bulk.

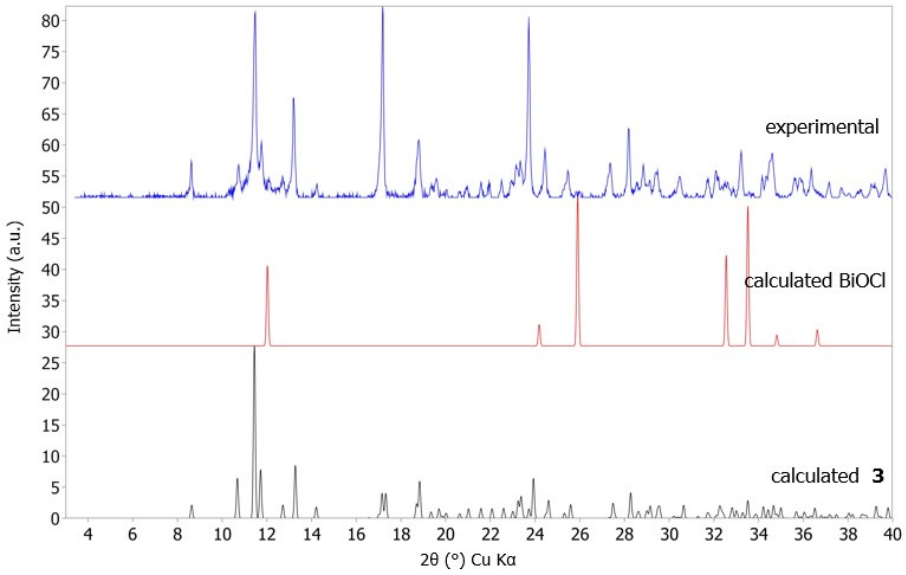

Figure S8. Powder X-ray diffraction data for the bulk product from the synthesis of bismuth chloride and terpy in the absence of H_2PDC overlaid with the calculated pattern generated from the crystallographic information file of **3** and BiOCl.

III. Luminescence Measurements

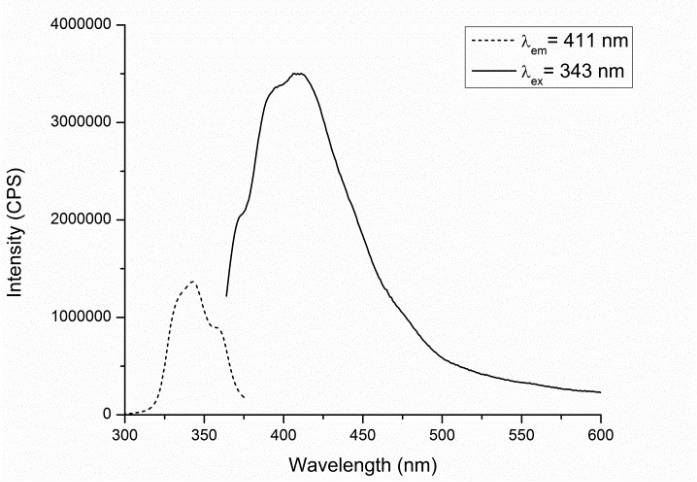

Figure S9. Room temperature excitation (dashed) and emission (solid) spectra for 2,6-pyridinedicarboxylic acid.

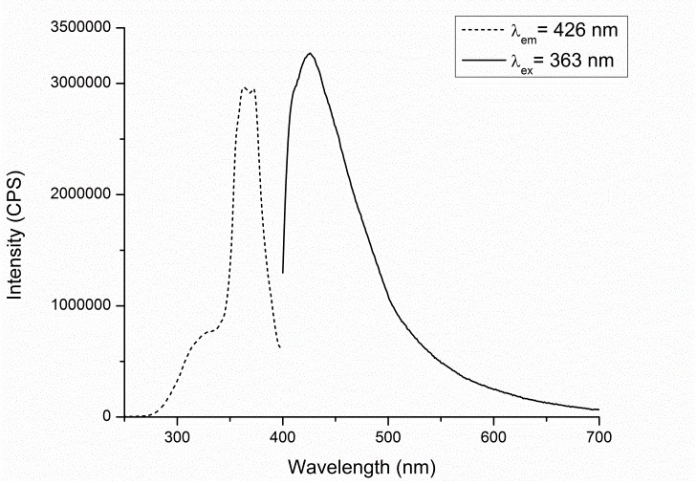

Figure S10. Room temperature excitation (dashed) and emission (solid) spectra for 1,10-phenanthroline.

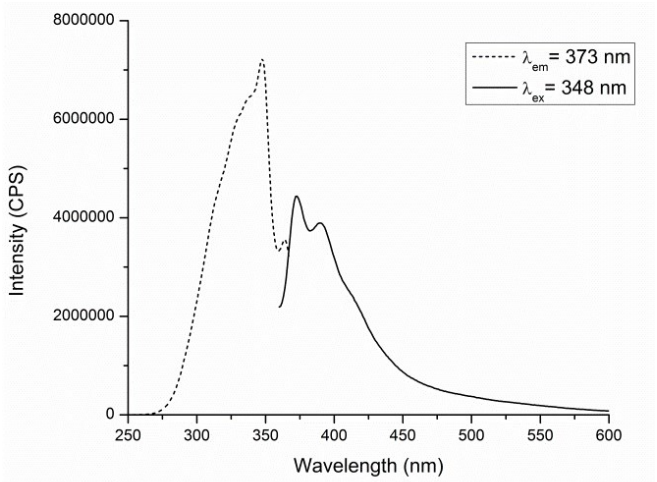

Figure S11. Room temperature excitation (dashed) and emission (solid) spectra for 2,2':6'2"-terpyridine.

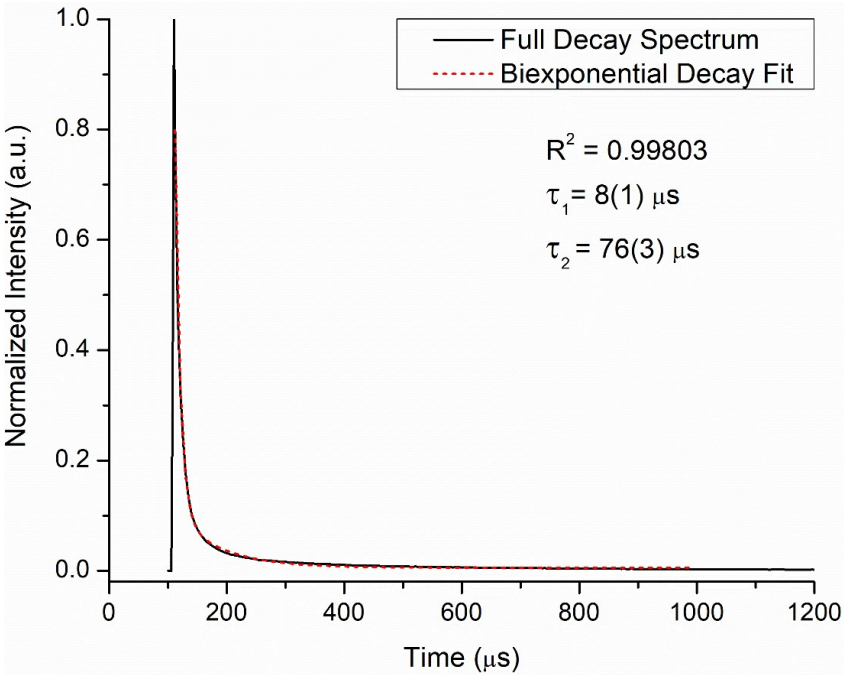

Figure S12. Lifetime decay curve of **1**; emission at 570nm upon irradiation at 387nm.

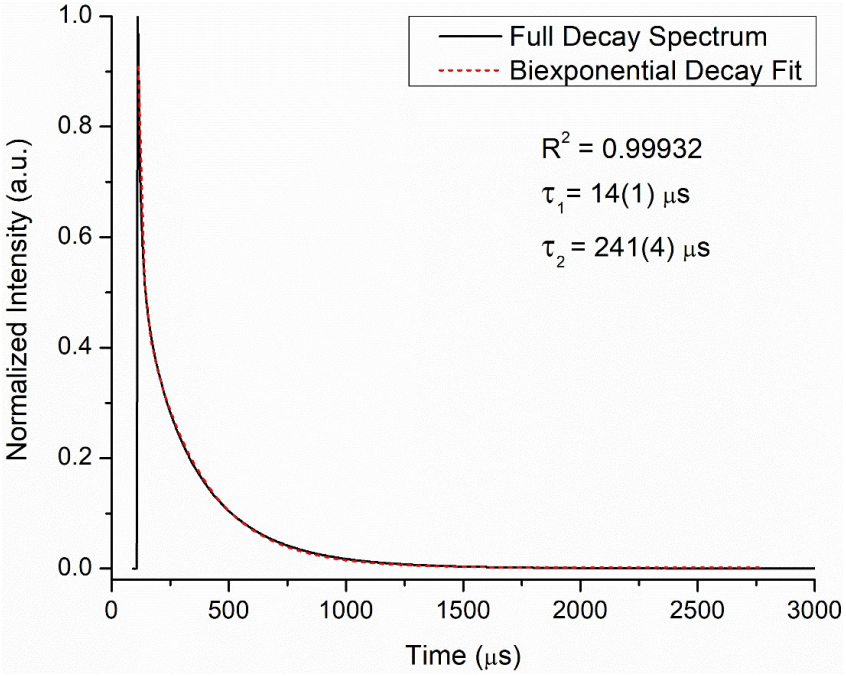

Figure S13. Lifetime decay curve of **2** emission at 537nm upon irradiation at 387nm.

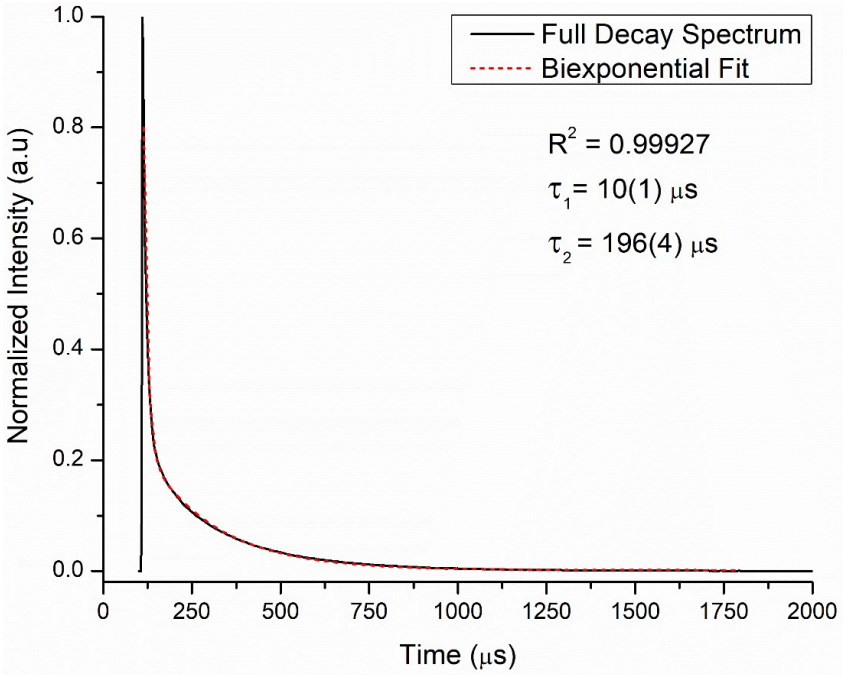

Figure S14. Lifetime decay curve of **3**; emission at 537nm upon irradiation at 387nm.

IV. UV-vis Absorption Spectroscopy

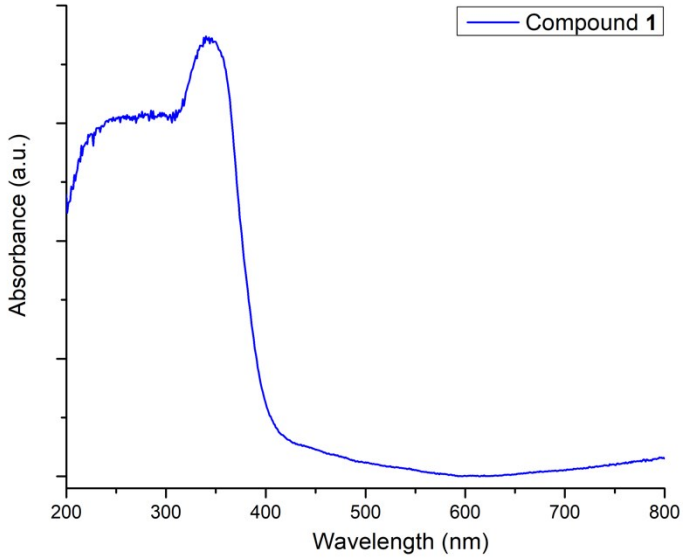

Figure S15. UV-vis absorption spectrum of **1**.

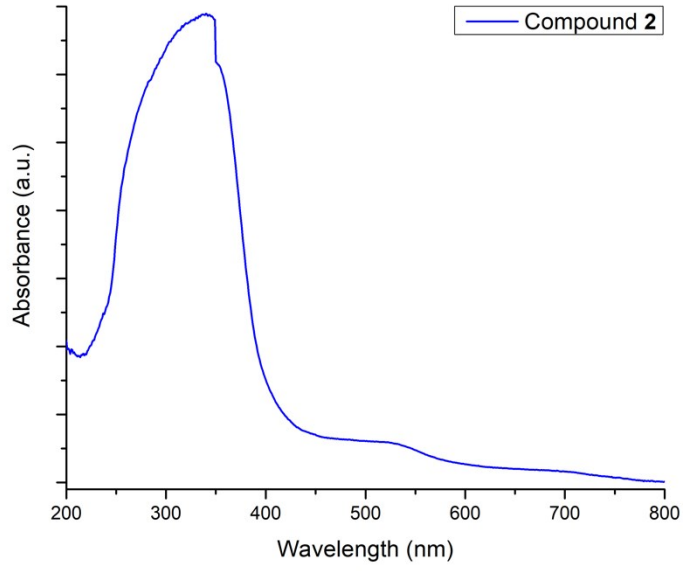

Figure S16. UV-vis absorption spectrum of **2**.

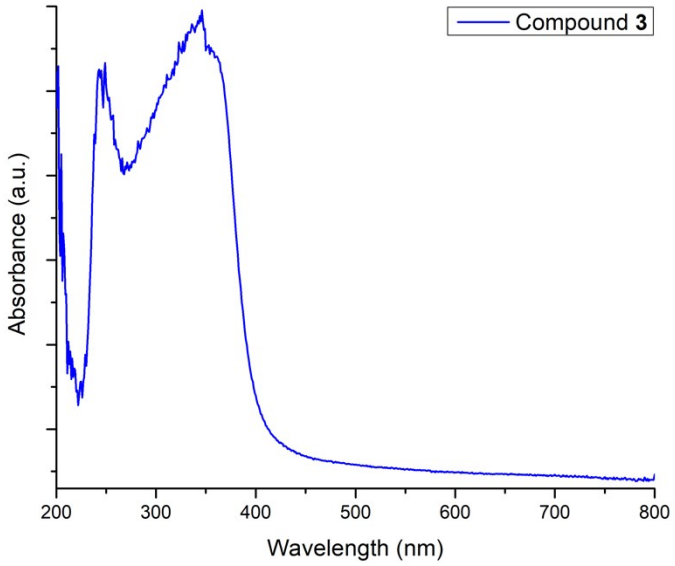

Figure S17. UV-vis absorption spectrum of **3**.

V. Thermogravimetric Analysis

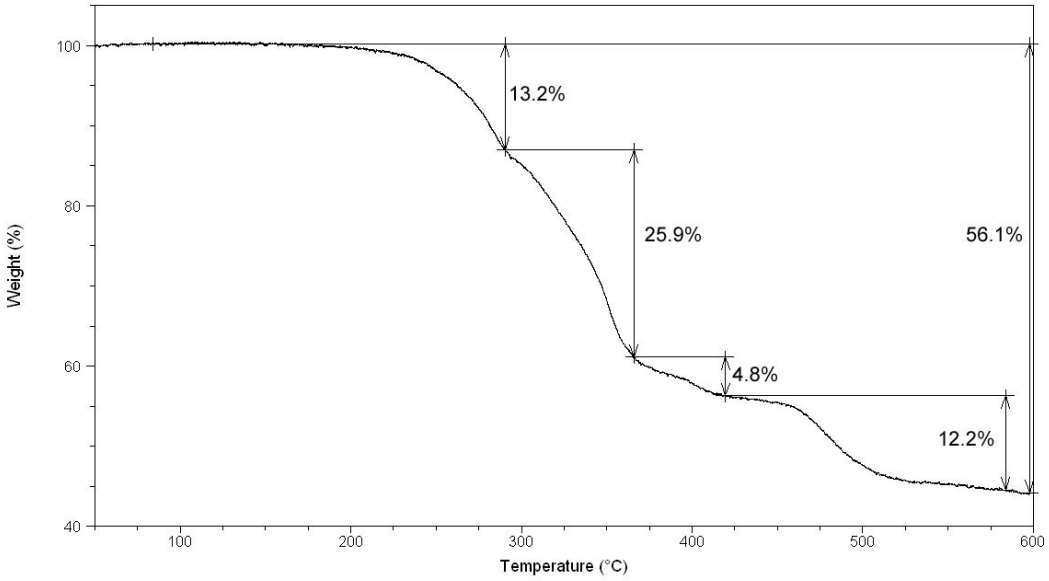

Figure S18. TGA plot for **1** collected over 50-600°C.

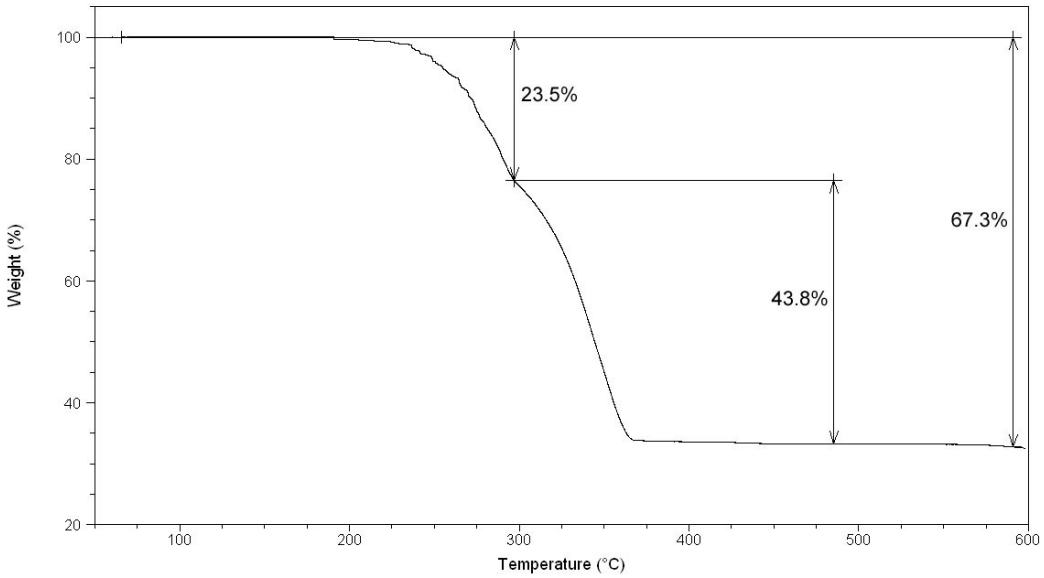

Figure S19. TGA plot for **3** collected over 50-600°C.

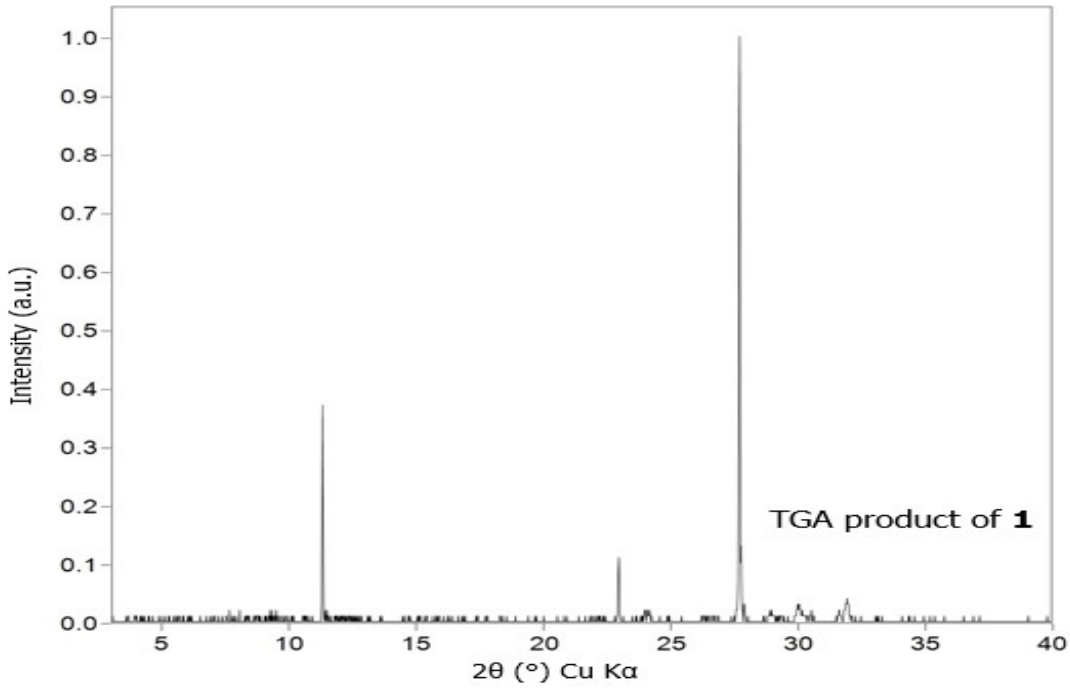

Figure S20. PXRD pattern of the thermal decomposition product of **1**. Attempts to index the peaks proved unsuccessful.

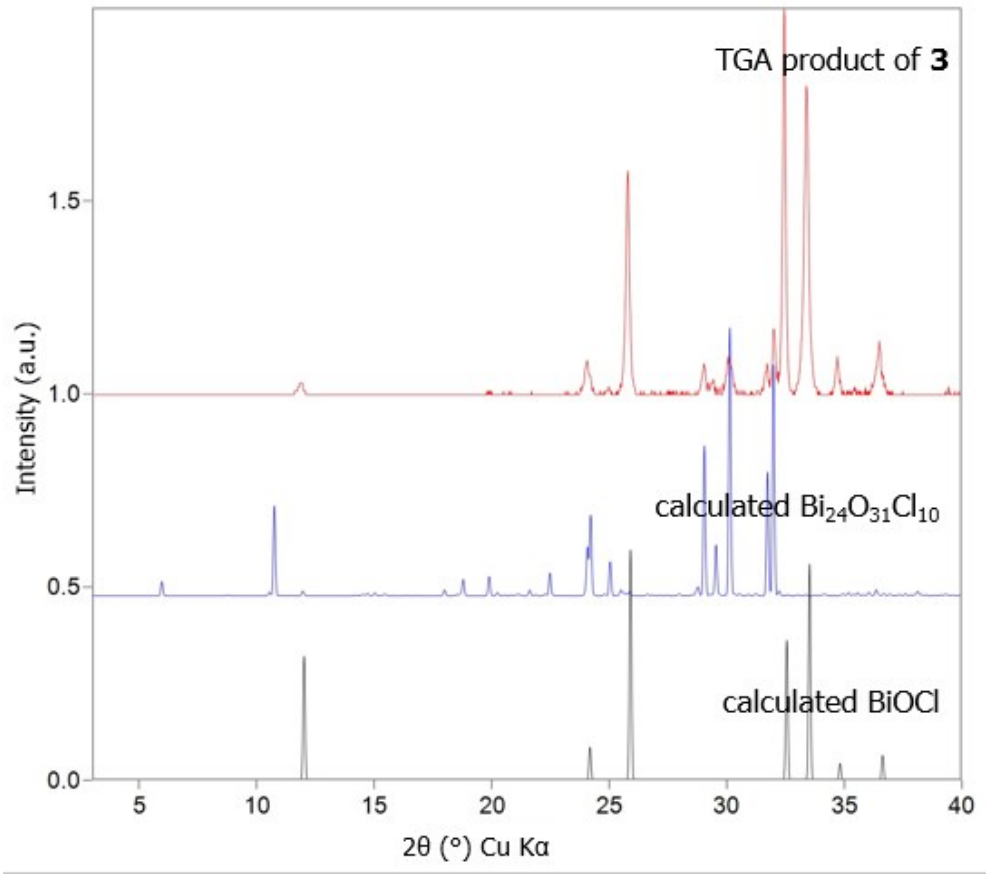

Figure S21. PXRD pattern of the thermal decomposition product of **3** overlayed with the crystallographic information file for BiOCl and $Bi_{24}O_{31}Cl_{10}$.

VI. Raman Spectra

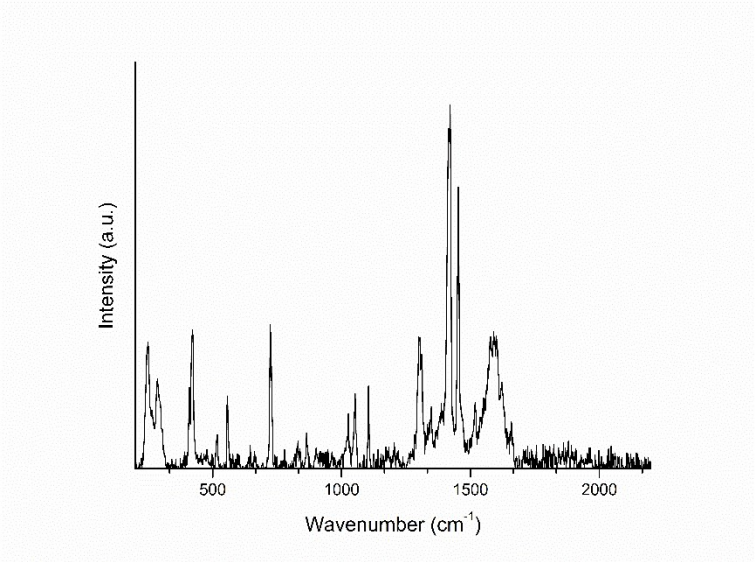

Figure S22. Raman spectrum for **1** shown over 200-2200 cm^{-1}.

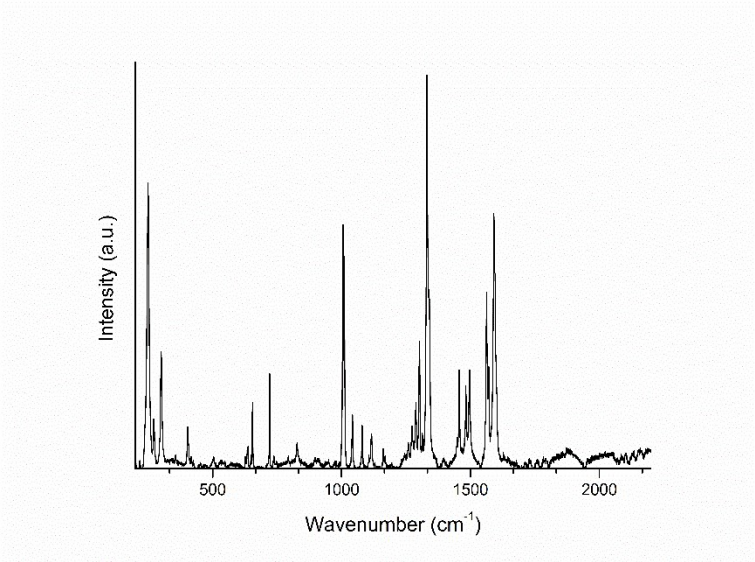

Figure S23. Raman spectrum for **3** shown over 200-2200 cm^{-1}.

VII. Computational Analysis

Influence of spin-orbit coupling on the low-lying bands in 2.

In order to quantify the effect of spin-orbit coupling (SOC) and its influence on the low-lying part of the spectra, the vertical spectra were computed with the slater-type TZP basis set[1] and the relativistic ZORA (Zeroth Other Relativistic Approximation) Hamiltonian either at the scalar relativistic level or the two-component level, [2-4] and with the CAM-B3LYP and PBE0 functional.[5-6] All the calculations were performed using the ADF package. [6-8] Twelve excited states were computed.

For the smaller compound **1**, $BiCl_3phen_2$, the low-lying bands were computed without and with SOC in order to quantify the necessity of including it or not. From Figure S24, one can observe in this case that SOC induces a shift and a broadening of the spectra. Some peaks around 450 nm are more intense, but the overall pictures remain the same. Thus, SOC was not considered.

Figure S24. Influence of spin-orbit coupling on the low-lying bands of the $BiCl_3phen_2$ monomer compound computed with the PBE0 and CAM-B3LYP functionals.

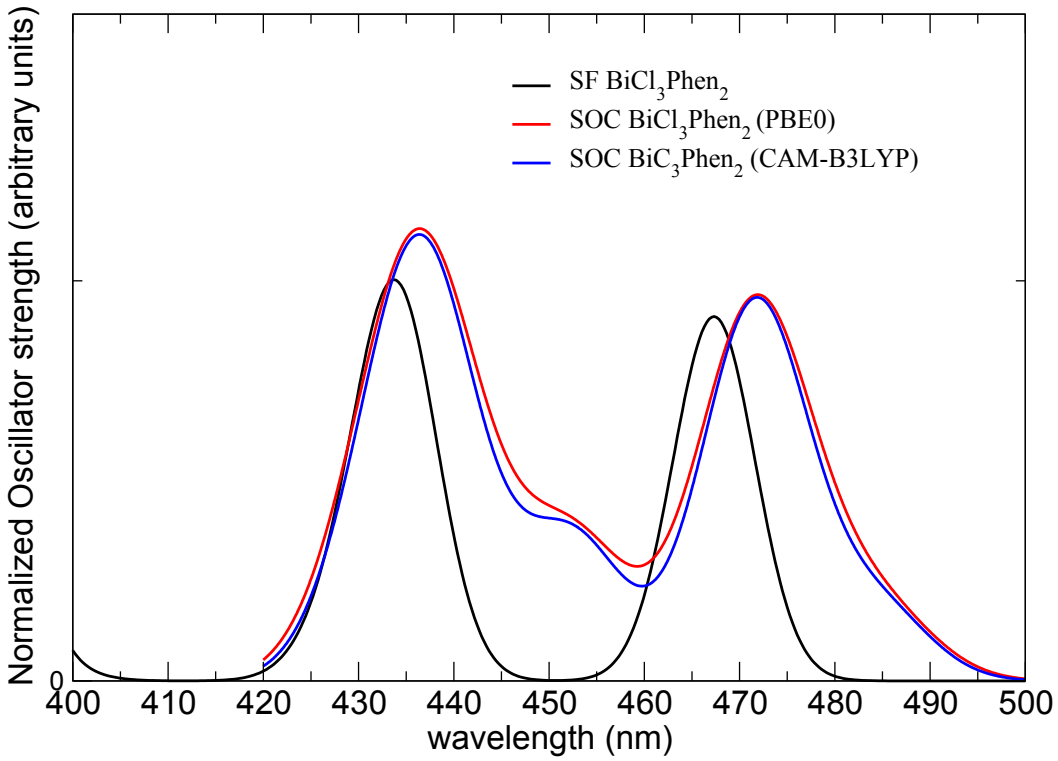

Table S1: Decomposition of the main singlet to singlet excitations of the $BiCl_3phen_2$ linear trimer and the tetramer species.

λ (nm)	Decomposition of the main singlet to singlet excitations for the trimer compound
420.0	0.97 (HOMO-2 → LUMO) -0.18 (HOMO-2→ LUMO+3)
410.7	0.67 (HOMO→ LUMO+1) -0.51 (HOMO-1→ LUMO+1) 0.32 (HOMO→ LUMO+4)
405.8	-0.58 (HOMO-1→ LUMO+1) -0.43 (HOMO→ LUMO+2) 0.38 (HOMO-1→ LUMO+5)
387.8	0.67 (HOMO-1→ LUMO+3) 0.58 (HOMO→ LUMO+4) -0.28 (HOMO-1→ LUMO+4)
386.7	-0.98 (HOMO-2→ LUMO+2) -0.18 (HOMO-2→ LUMO+1)
373.5	0.66 (HOMO→ LUMO+5) -0.55 (HOMO-1→ LUMO+5) 0.28 (HOMO→ LUMO+4)
370.2	0.65 (HOMO-1→ LUMO+6) 0.58 (LUMO→ LUMO+6) -0.21 (HOMO→ LUMO+4)
368.3	0.94 (HOMO-2→ LUMO+7) -0.21 (HOMO-2→ LUMO+6) -0.13 (HOMO-1→ LUMO+9)
352.4	-0.65 (HOMO→ LUMO+9) 0.55 (HOMO-1→ LUMO+9) -0.32 (HOMO→ LUMO+7)
λ (nm)	Decomposition of the main singlet to singlet excitations for the tetramer compound
415.6	-0.51 (HOMO-1→ LUMO+7) -0.45 (HOMO-1→ LUMO+5) 0.41 (HOMO→ LUMO+6)
380.7	0.66 (HOMO-1→ LUMO+9) 0.65 (HOMO→ LUMO+10) -0.19 (HOMO→ LUMO+7)
376.4	-0.67 (HOMO-2→ LUMO) 0.66 (HOMO-3→ LUMO+1) -0.21 (HOMO-2→ LUMO+1)
371.5	-0.68 (HOMO→ LUMO+12) 0.61 (HOMO-1→ LUMO+13) 0.28 (HOMO-1→ LUMO+11)
356.4	-0.44 (HOMO-2→ LUMO+2) 0.37 (HOMO-3→ LUMO+5) 0.36 (HOMO-3→ LUMO+3)

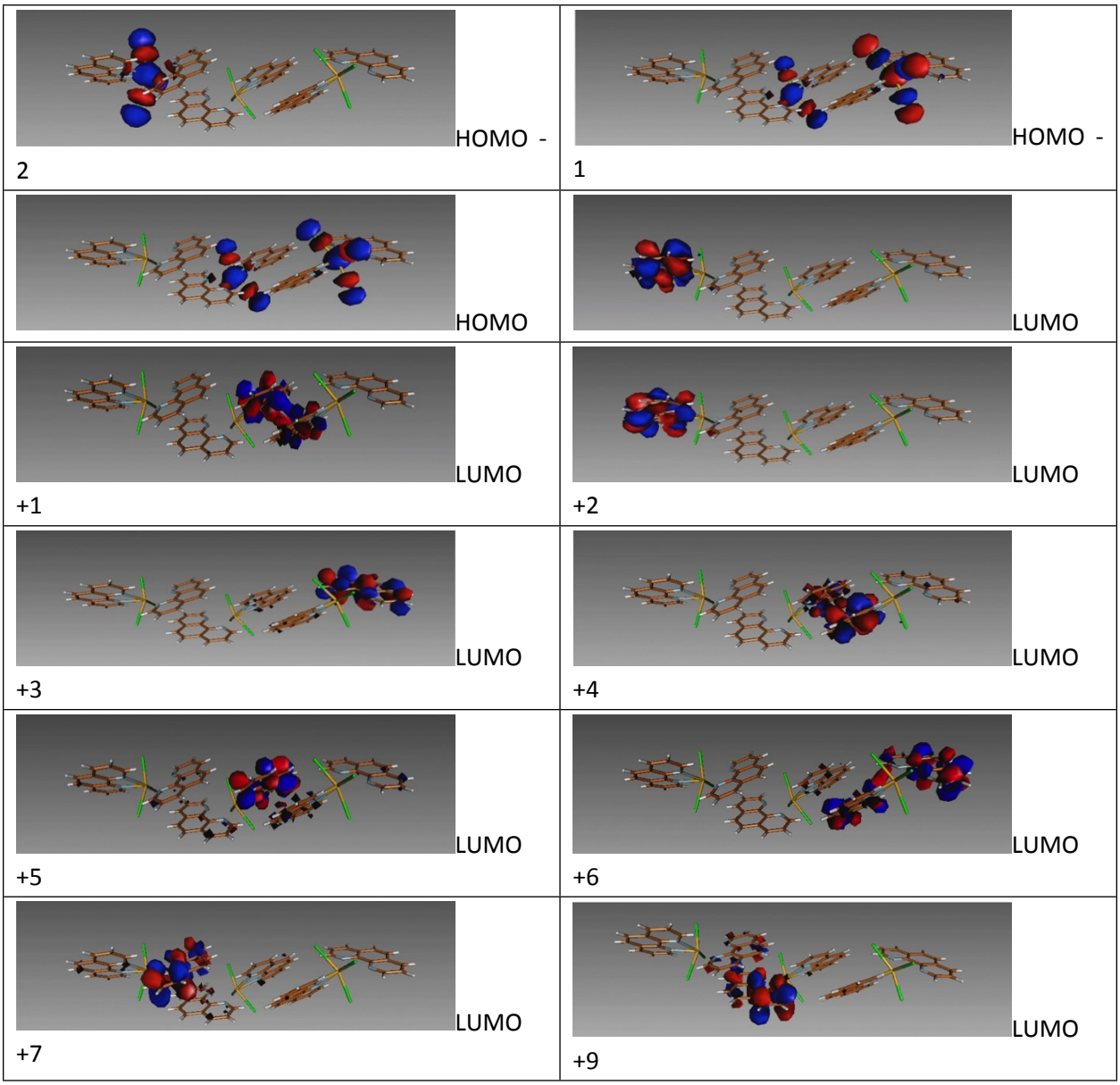

Figure S25. Molecular Orbitals implied in the main first excitations of the BiCl3phen2 linear trimer compound.

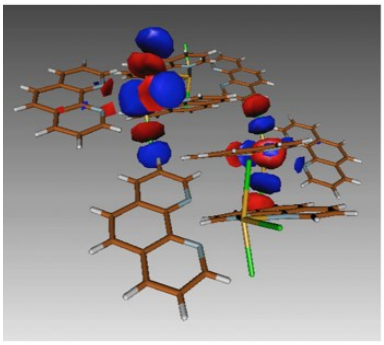 HOMO-3	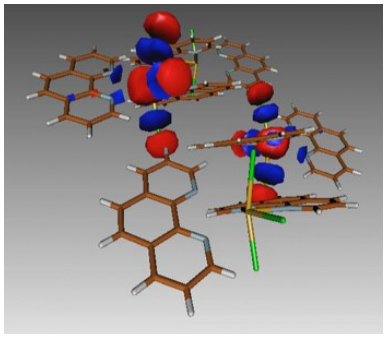 HOMO-2	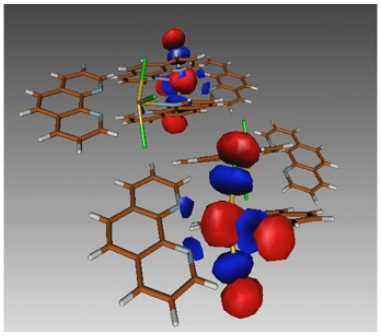 H OMO-1
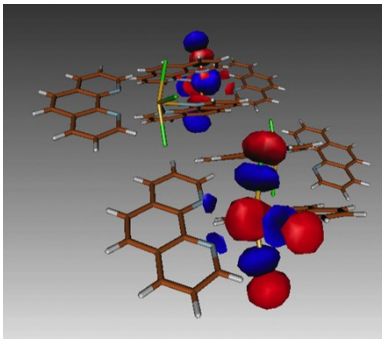 HOMO	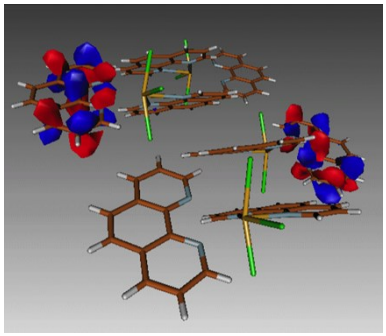 LUMO	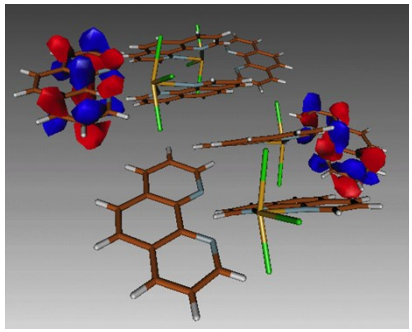 LUMO +1
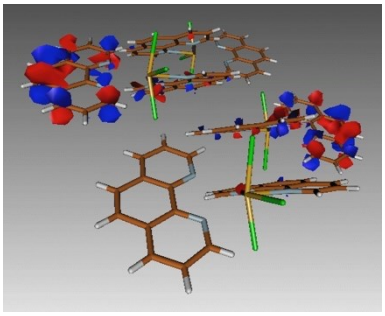 LUMO +2	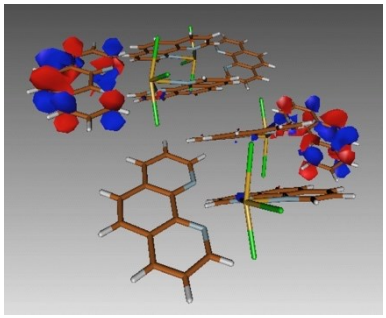 LUMO +3	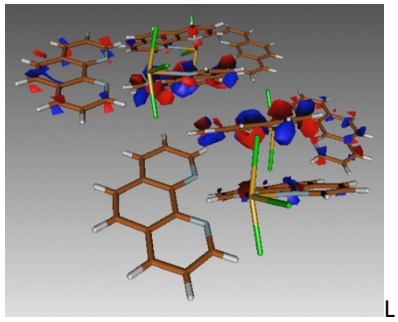 L UMO +4
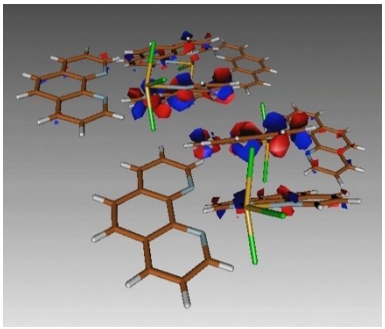 LUMO +5	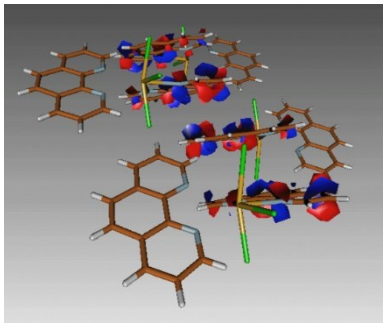 LUMO +6	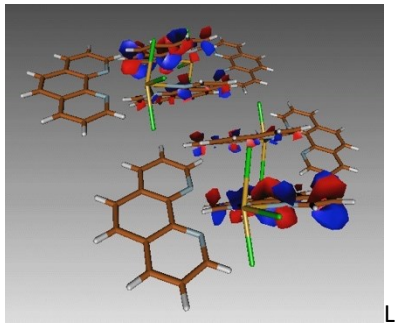 L UMO +7

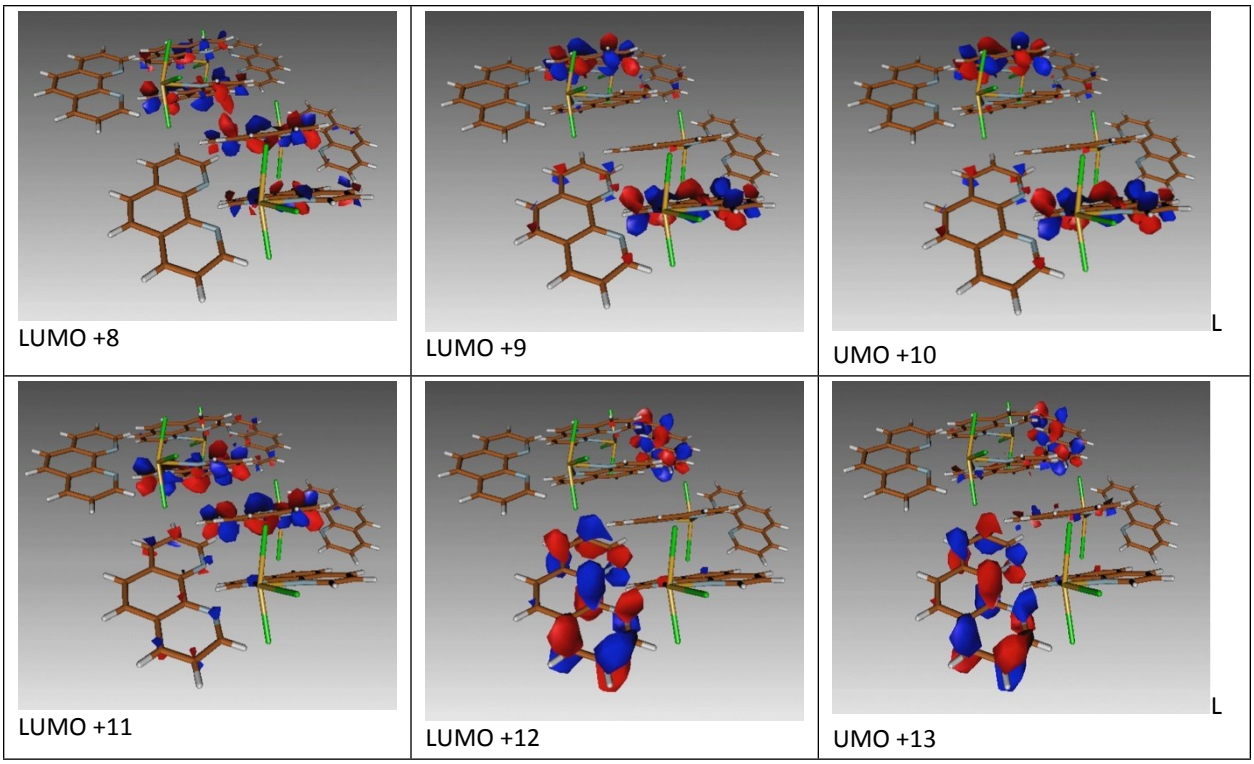

Figure S26. Molecular Orbitals implied in the main first excitations of $BiCl_3phen_2$ tetrameric compound

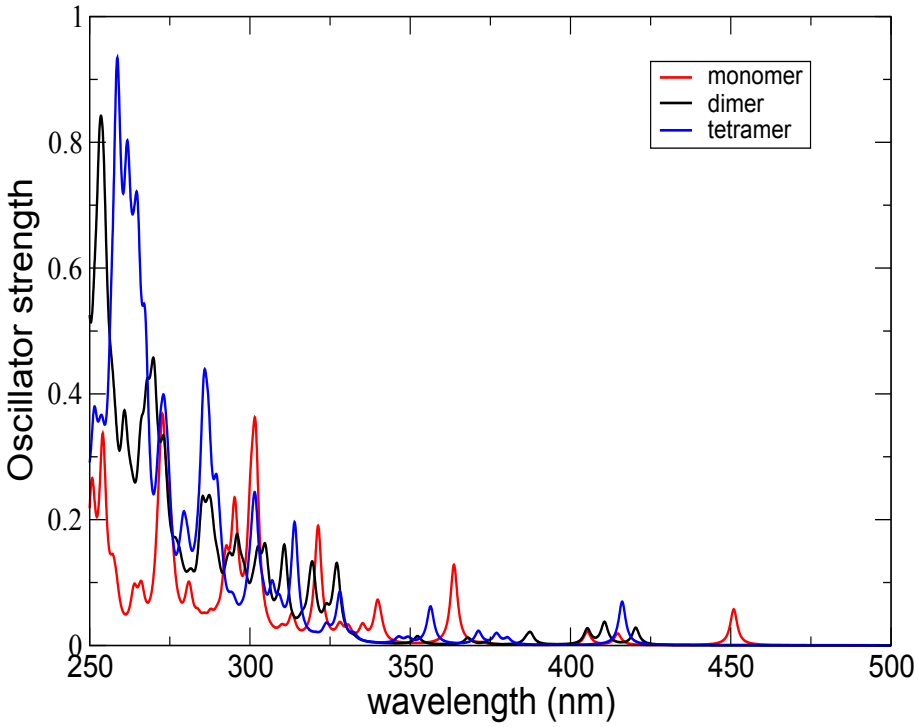

Figure S27: Computed absorption spectra of the $BiCl_3phen_2$ compound for the monomer, trimer and tetramer. Unnormalized spectra.

Table S2. Decomposition of the strongest singlet to singlet excitations of the Bi_2Cl_6 ter_2 tetramer compound above 380 nm. To justify the selection of the main three states, the oscillator strength computed is at least 10 times higher than the other transitions.

λ (nm)	Decomposition of the main singlet to singlet excitations
427.1	
411.4	0.87 (HOMO-6 → LUMO+6) -0.42 (HOMO-6→ LUMO+4) -0.14 (HOMO-9→ LUMO+6)
404.9	
403.9	
397.1	
395.4	-0.79 (HOMO-15→LUMO+1) -0.47 (HOMO-10→ LUMO+1) -0.29 (HOMO-14→ LUMO+1)
391.0	
390.7	

387.8	-0.59 (HOMO-14→ LUMO+2) -0.52 (HOMO-11→ LUMO+2) -0.30 (HOMO-13→ LUMO+2)
383.9	
383.4	
382.5	
382.3	
380.0	
374.1	
371.0	
367.6	
363.5	
363.3	
362.3	

In Table S3, singlet and triplet states are reported for the ^{BiCl_3phen_2} tetramer ($^{Bi_4Cl_{12}phen_8}$), ^{Bi_4Cl_8PDC_2phen_4} dimer ($^{Bi_8Cl_{16}PDC_4phen_8}$) and ^{Bi_2Cl_6ter_2} tetramer compounds ($^{Bi_8Cl_{12}ter_8}$), respectively. Regarding the three spectra, one can see that for the two first compounds, there is a discontinuity of states in the low-wavelength part with a gap about 30 nm, while the ^{Bi_2Cl_6ter_2} absorption spectrum is almost continuous. This is a proof of the singularity of the later compound with respect to the two others.

Table S3. Lowest absorption wavelengths of singlet and triplet states (nm) of the $BiCl_3phen_2$ tetramer, $Bi_4Cl_8PDC_2phen_4$ dimer and $Bi_2Cl_6ter_2$ tetramer compounds.

$BiCl_3phen_2$		$Bi_4Cl_8PDC_2phen_4$		$Bi_2Cl_6ter_2$	
Triplets	Singlets	Triplets	Singlets	Triplets	Singlets
419.4	415.6	402.6	398.4	427.3	427.1
419.4	415.5	401.3	397.2	417.5	411.4
381.2	380.7	369.4	366.2	408.1	404.9
381.2	380.7	360.8	360.7	408.1	403.9
377.6	376.4	359.9	356.6	400.9	397.1
377.6	376.4	349.7	349.6	399.9	395.4
373.2	371.5	330.8	330.4	394.5	391.0
373.2	371.5	329.2	329.1	391.0	390.7

359.4	356.4	322.9	322.9	390.5	387.8
359.4	356.4	317.7	308.8	384.0	383.9

REFERENCES

1. Van Lenthe, E.; Baerends, E. J., Optimized Slater-type basis sets for the elements 1–118. *J. Comput. Chem.* **2003,** *24* (9), 1142-1156.
2. Van Lenthe, E. ; Baerends, E. J.; Snijders, J. G., Relativistic regular two-component Hamiltonians. *The J. Chem. Phys.* **1993,** *99* (6), 4597-4610.
3. Van Lenthe, E.; Baerends, E. J.; Snijders, J. G., Relativistic total energy using regular approximations. *J. Chem. Phys.* **1994,** *101* (11), 9783-9792.
4. Sadlej, A. J.; Snijders, J. G.; Van Lenthe, E.; Baerends, E. J., Four component regular relativistic Hamiltonians and the perturbational treatment of Dirac's equation. *J. Chem. Phys.* **1995,** *102* (4), 1758-1766.
5. Yanai, T.; Tew, D. P.; Handy, N. C., *Chem. Phys. Lett* **2004,** *393*, 51-57.
6. Perdew, J. P.; Ernzerhof, M.; Burke, K., Rationale for mixing exact exchange with density functional approximations. *J. Chem. Phys.* **1996,** *105* (22), 9982-9985.
7. te Velde, G.; Bickelhaupt, F. M.; Baerends, E. J.; Fonseca Guerra, C.; van Gisbergen, S. J. A.; Snijders, J. G.; Ziegler, T., Chemistry with ADF. *J. Comput. Chem.* **2001,** *22* (9), 931-967.
8. Fonseca Guerra, C.; Snijders, J. G.; te Velde, G.; Baerends, E. J., Towards an order-N DFT method. *Theo. Chem. Acc.* **1998,** *99* (6), 391-403.
9. Baerends, E. J.; Ziegler, T.; A.J. Atkins; J. Autschbach; O. Baseggio; D. Bashford; A. Bérces; F.M. Bickelhaupt; C. Bo; P.M. Boerrigter; L. Cavallo; C. Daul; D.P. Chong; D.V. Chulhai; L. Deng; R.M. Dickson; J.M. Dieterich; D.E. Ellis; M. van Faassen; L. Fan, T. H. F.; C. Fonseca Guerra; M. Franchini; A. Ghysels; A. Giammona; S.J.A. van Gisbergen; A. Goez; A.W. Götz; J.A. Groeneveld; O.V. Gritsenko; M. Grüning; S. Gusarov; F.E. Harris; P. van den Hoek; Z. Hu; C.R. Jacob; H. Jacobsen; L. Jensen; L. Joubert; J.W. Kaminski; G. van Kessel; C. König; F. Kootstra; A. Kovalenko; M.V. Krykunov; E. van Lenthe; D.A. McCormack; A. Michalak; M. Mitoraj; S.M. Morton; J. Neugebauer; V.P. Nicu; L. Noodleman; V.P. Osinga; S. Patchkovskii; M. Pavanello; C.A. Peeples; P.H.T. Philipsen; D. Post; C.C. Pye; H. Ramanantoanina; P. Ramos; W. Ravenek; J.I. Rodríguez; P. Ros; R. Rüger; P.R.T. Schipper; D. Schlüns; H. van Schoot; G. Schreckenbach; J.S. Seldenthuis; M. Seth; J.G. Snijders; M. Solà; M. Stener; M. Swart; D. Swerhone; V. Tognetti; G. te Velde; P. Vernooijs; L. Versluis; L. Visscher; O. Visser; F. Wang; T.A. Wesolowski; E.M. van Wezenbeek; G. Wiesenekker; S.K. Wolff, T.; .K. Woo; Yakovlev, A. L. Vrije Universiteit, Amsterdam, The Netherlands, http://www.scm.com. , 2019.
10. Bowmaker, G. A.; Hannaway, F. M. M.; Junk, P. C.; Lee, A. M.; Skelton, B. W.; White, A. H., Synthetic, Structural and Vibrational Spectroscopic Studies in Bismuth(III) Halide/N,N'-Aromatic Bidentate Base Systems. V Bismuth(III) Halide/N,N'-Bidentate Ligand (1 : 2) Systems. *Australian Journal of Chemistry* **1998,** *51* (4), 325-330.